Markov Latent Frequency Transition Analysis for Robust Bearing Diagnosis in Transient Noise Scenarios

Junxiao Ma

College of Engineering, Shantou University, Shantou, Guangdong, China lanyerking@vip.qq.com

Peng Chen^{1,2,*}

¹College of Engineering, Shantou University, Shantou,
Guangdong, China

²Key Laboratory of Intelligent Manufacturing
Technology, Ministry of Education of China, Shantou,
Guangdong, China
pengchen@alu.uestc.edu.cn

Changbo He
College of Electrical Engineering and Automation, Anhui
University, Hefei, China.
changbh@ahu.edu.cn

Abstract—In real-world applications, the diagnostic accuracy of rolling bearings is often compromised by environmental factors such as variable rotational speeds, transient noises, and unexpected mechanical impacts. These factors can obscure damage symptoms, making precise detection of bearing failures challenging. Conventional diagnostic methods struggle to handle these complexities and often miss failure features hidden in multifaceted random transient noise. To address these issues, this research introduces the Markov Latent Frequency Transition Peak Rate (MLFTPR) methodology. MLFTPR focuses on accurately monitoring temporal state transitions and identifying anomalous signals, aiming to mitigate transient noise at the source and improve resistance to external disturbances. This enhances precision and reliability in demodulation band selection. Additionally, an amplitude interference-reduction feature is integrated to recognize and suppress transient noise effectively. Experimental results validate the efficacy of MLFTPR, demonstrating its capability to accurately diagnose bearing defects even amidst transient disturbances.

Keywords-ball bearings; fault diagnosis; prognostics and health management; vibration signal analysis; transient noise; anomaly detection. Yuhao Wu College of Engineering, Shantou University, Shantou, Guangdong, China 507663149@qq.com

Chengning Zhou
Nuclear Power Institute of China, Chengdu, China.
chengningzhou@foxmail.com

Qingsheng Wei College of Engineering, Shantou University, Shantou, Guangdong, China wei2311295448@163.com

I. INTRODUCTION

Rolling bearings are widely used in various industries, acting as key components in mechanical equipment across manufacturing, transportation, and energy production. However, due to long-term operation and harsh working conditions, rolling bearings are prone to wear, cracks and other failures, which can degrade equipment performance or cause shutdowns. Therefore, timely and accurate monitoring and diagnosis rolling bearings are crucial for ensuring the safe and stable operation of mechanical systems [1], [2].

The primary methods for detecting and diagnosing rolling bearing faults including vibration signal analysis [3], [4], [5] and deep learning-based approaches [7], [8]. Vibration signal analysis focuses on extracting key features in the tine and frequency domains to evaluate bearing faults, making it effective with limited data and widely applicable. Conversely, deep learning methods, such as Convolutional Neural Networks (CNNs) [6], Transformers [7], rely on complex algorithms and large amounts of datasets to uncover intricate patterns and nonlinear relationships in vibration signals. However, these methods often suffer from poor interpretability and require substantial data and computing resources.

52305085), the Guangdong Basic and Applied Basic Research Foundation (Grant 2022A1515010859), the Shantou University (STU) Scientific Research Initiation Grant (Grant NTF21029), and the Original Innovation Grant Project of the Nuclear Power Institute of China (Grant YF23051).

^{*} Corresponding author: Peng Chen (pengchen@alu.uestc.edu.cn or dr.pengchen@foxmail.com)

This research has been partially funded by several sources, including the National Natural Science Foundation of China (Grants 52105111 and

In industrial environments, the vibration signals from localized damage to rolling bearings are crucial for fault diagnosis. Such signals typical feature repetitive transients due to periodic impacts from localized defects in rotating components [8]. These impacts have noticeable periodic and transient characteristics, visible in the frequency domain, and can indicate damage in components like the inner ring, outer ring and rolling elements. A significant challenge in bearing fault detection and diagnosis is distinguishing fault information from environmental noise to accuracy identify fault characteristic frequencies [9].

To address this challenge, Antoni et. al. [10] applied Spectral Kurtosis (SK) due to its effectiveness in detecting and characterizing early faults despite strong masking noise. They also proposed the Kurtogram, employing the Short-time Fourier Transform (STFT) to identify transient faults, such as early bearing or gear damage, by analyzing both frequency and time domains. Additionally, the Square Envelope Spectrum (SES) method was introduced, utilizing the Hilbert transform to create an analytical signal, extract its envelope, and square it to enhance periodic components. Antoni et al. [11] also developed the Fast Kurtogram (FK), which reduces computation time through fast filter banks and efficiently detects and characterizes transient signals. Continuing these advancements, Lei et al. [12] proposed an improved Kurtogram using wavelet packet transform (WPT) instead of STFT, significantly enhancing the sensitivity and accuracy of rolling bearing fault diagnosis through adaptive filtering and multi-scale analysis. To address the limitations of SES in detecting second-order cyclostationary (CS2) components, Borghesani et al. [13] introduced the Logarithmic Envelope Spectrum (LES), which remains unbiased amidst multiple CS2 spectral correlation sources. However, traditional SK methods face issues such as high sensitivity to impulse noise and limited ability to detect repetitive transient signals, often leading to misdiagnoses. Therefore, improved SK methods have been proposed. Barszcz et al. [14] developed the Protugram, selecting the optimal frequency band for vibration signal demodulation based on the kurtosis of the envelope spectrum amplitude, improving performance under strong non-Gaussian noise. Chen et al. [15] introduced the Product Envelope Spectrum (PES) and PESOgram to enhance the robustness of PES for fault diagnosis in the presence of diverse interference noises. Antoni et al. [16] addressed Kurtogram's limitations under noisy conditions by combining spectral entropy from time and frequency domains to create tools such as Squared Envelope (SE) Infogram and capturing SES Infogram, signal characteristics comprehensively. Li et al. [5] proposed the Multiscale Clustering Grey Infogram (MCGI), enhancing frequency band segmentation through hierarchical clustering to improve practical effectiveness.

Despite these advancements, traditional methods still struggle in environments with random impulse noise, lacking the robustness to identify potential transient interference frequencies. This research proposes a novel strategy to reduce transient noise interference in non-stationary bearing signals. It leverages the characteristic response of bearings to transient noise, identifying and suppressing minimal transient impact interference. By incorporating a Markov transfer matrix with

wavelet transform and signal reconstruction, this approach locates and suppresses abnormal signal components, enhancing the Kurtogram method's ability to determine the unique frequency band of bearing faults. Experimental evidence demonstrates that our method effectively diagnoses bearing faults even in the presence of transient noise.

II. RELATED THEORY

This section revisits the principal metric used for identifying signal transformations, which detects signal anomalies through analyzing local peak ratios, energy levels, and zero crossing rates. Techniques like Short-time Energy (STE)[17], Short-time Kurtosis (STK)[18], and Short-time Zero Crossing Rate (STZCR)[17], [19].

Consider a real-world discrete signal represented by a time series $[x_n]$, with indices ranging from 1 to N. Calculations for this signal are performed using the following parameters, where m is the time index, f represents the frame index, and h is the sliding window length. A window function, typically a rectangular window w, ensures uniform sample weighting within each frame.

$$x_f[m] = x[m + f \cdot h] \cdot w[m] \tag{1}$$

Local peaks within the signal's sliding window are pinpointed, with a sample qualifying as a peak if it exceeds the values of its immediate neighbors. This peak detection can be mathematically expressed as follows.

$$x[m] - x[m-1] > 0,$$

 $x[m+1] - x[m] \le 0$ (2)

To accurately detect peaks that indicate signal changes, it is essential to consider both the magnitude and the rate of variation. Focusing solely on amplitude, as is done with STE, STK, and STZCR, might miss significant dynamics in the signal. By introducing a threshold m_d , peak detection is improved in noisy environments, allowing for better tracking of signal shifts and more effective identification of anomalies.

$$x[m] - x[m-1] > m_d,$$

 $x[m+1] - x[m] \le m_d$ (3)

Filtered conditional peaks (Np) with a moving window are counted, and the Short-Term Local Peak Rate (STLPR) is defined as the ratio of these peaks to the total samples in the window.

$$STLPR = \frac{N_p}{M} \tag{4}$$

where *M* denotes the window function's length.

The assessment of peaks within a moving window employ (4), a metric that quantifies anomaly density in the signal, thereby capturing its local characteristics over the duration of the window.

III. PROPOSED METHOD

Choosing the appropriate conditional peak threshold m_d is vital for STLPR accuracy. Manual setting can lead to inconsistencies, especially with transient non-Gaussian noise.

To address this, a Markov Latent Frequency Transition Peak Rate (MLFTPR) is proposed. This method encompasses signal preprocessing, Markov modeling for state change tracking, and interference suppression for signal differentiation.

A. Wavelet Analysis and Environmental Noise Suppression

The Daubechies Wavelet Transform (DWT) [20], [21] is employed due to its smoothness and effective time-frequency localization, which aids in transient detection. For a vibration signal x(t), DWT provides approximation coefficients $(cA_{j,k})$ and detail coefficients $(cD_{j,k})$.

$$x = \sum_{k=-\infty}^{+\infty} cA_{j,k} \phi_{j,k}(t) + \sum_{k=-\infty}^{+\infty} cA_{j,k} \psi_{j,k}(t)$$
 (5)

where j signifies the scale factor of the wavelet, and k represents its shift factor, determining the central position. $\phi_{j,k}$ represents the scaling function, while $\psi_{j,k}$ corresponds to the scale function.

In the decomposition process of DWT, higher-level approximation and detail coefficients are sequentially derived from each approximation stage, preserving and recovering signal features across multiple frequencies and scales until the desired decomposition depth is achieved. This procedure can be mathematically represented as follows:

$$cA_{j,k} = \sum_{n} h[n-2k]x_{j-1,n}$$

$$cD_{j,k} = \sum_{n} g[n-2k]x_{j-1,n}$$
(6)

where h[n] and g[n] are the low-pass and high-pass filters, respectively. The variable $x_{j-1,n}$ represents the lower frequency component of the current approximation, embodying the broad and sustained characteristics of the signal.

Next, the approximation and detail coefficients undergo refinement through thresholding and filtering. The filtered approximation coefficients, denoted as cA', are obtained by applying a Butterworth filter, mathematically described as below.

$$cA'_{n} = \sum_{i=0}^{M} b_{i} \cdot cA_{n-i} - \sum_{j=1}^{N} a_{j} \cdot cA'_{n-j}$$
 (7)

For (7), b_i and a_i are the feed-forward coefficients of the filter, respectively. The index j starts at 1, given that a_0 is commonly normalized to 1.

Soft-thresholding is applied to the detail coefficients, denoted as cD', at each stage of the decomposition to mitigate noise, as shown below.

$$cD_{i}^{'} = \begin{cases} \operatorname{sgn}(cD_{i})(|cD_{i}| - \varepsilon) & |cD_{i}| \ge \varepsilon \\ 0 & |cD_{i}| < \varepsilon \end{cases}$$
(8)

The threshold ε is determined as a specific percentage of the maximum value of cD_i , described by the following equation.

$$\varepsilon = k \cdot \max(cD_i) \tag{9}$$

After post-processing the approximation and detail coefficients, the Inverse Discrete Wavelet Transform (IDWT) synthesizes them to retrieval a refined signal. This process helps in preserving the essential details of the signal after noise or disturbance removal. The signal recovery is mathematically represented as follows.

$$\hat{x}(t) = \sum_{i = -\infty}^{\infty} \left(cA'_{j,k} \phi_{j,k}(t) + \sum_{k = -\infty}^{\infty} cD'_{j,k} \psi_{j,k}(t) \right)$$
(10)

where $\phi_{j,k}(t)$ and $\psi_{j,k}(t)$ are the scaling and wavelet functions, respectively, incorporating scale and shift parameters (j, k). It is essential to preserve peaks that significantly deviate the mean of the original signal. This set of peaks is identified by indices that satisfy the following condition.

$$\Pi = \{ i \mid x_i(t) > \tau \forall x_i(t) < -\tau, i \in \{1, \dots, |n|\} \}$$
 (11)

where τ represents the mean of the original signal. The identification of peaks within a reconstructed signal is then defined by the following equation.

$$\hat{x}_{i}'(t) = \begin{cases} x_{i}(t), & \text{if } i \in \Pi \\ \hat{x}_{i}(t), & \text{if } i \notin \Pi \end{cases}$$
 (12)

B. Markov Chain Analysis and Signal State Modeling

A Markov model subsequently employed to statistically describe the transitions between states in the reconstructed signal. This model posits that the next state is depend solely on the current state, independent of prior states. This concept is formally represented by the follows.

$$P(x_i \mid x_{i-1}, x_{i-2}, \dots, x_1) = P(x_i \mid x_{i-1})$$
 (13)

where the transition to the next state, denoted as x_i , is determined exclusively by the probability associated with the current state, x_{i-1} . This indicates that the likelihood of moving to the next state is entirely dictated by the immediately preceding state, with no influence from earlier states in the sequence.

In the context of Markov chains, each state transition is defined probabilistically, with the system's current state dependent solely on its preceding state, a property referred to as the Markov property. This property implies that future states are independent of past states given the present state. This transition behavior is mathematically captured in a transition probability matrix, which enumerates the conditional probabilities for transitions between all possible pairs of states. For a system with n-state, this matrix provides a comprehensive view of the n^2 potential state transitions, formulated through a specific computational method. The matrix is structured as follows:

$$M_{TPM} = \begin{bmatrix} p_{11} & p_{12} & \cdots & p_{1j} & \cdots \\ p_{21} & p_{22} & \cdots & p_{1j} & \cdots \\ \vdots & \vdots & & \vdots & & \vdots \\ p_{i1} & p_{i2} & \cdots & p_{ij} & \cdots \\ \vdots & \vdots & \vdots & \vdots & & \end{bmatrix}$$
(14)

C. Signal State Mapping and Transition Frequency Calculation

The method integrates wavelet reconstruction to convert signal amplitudes into indexed intervals, labeled as j, which helps in identifying signal states S_i . This approach effectively differentiates normal states from anomalies. The conversion of complex continuous signals into a discrete format, as outlined (15), ensures the preservation of state transition integrity. The transformation of amplitudes into interval indices is governed by the following equation:

$$S_{i} = \begin{cases} j, & x_{n}[i] \in S_{j} \\ j, & x_{n}[i] = \max(x_{n}), j = n_{\text{bin}} - 1 \end{cases}$$
 (15)

The original signal is divided into states S_j , specifically into 10 bins ($n_{\text{bin}} = 10$), facilitating detailed state representation in the Markov model.

$$S_{j} = \left[\min(x_{n}) + (j-1) \cdot \Delta, \min(x_{n}) + j \cdot \Delta\right]$$

$$\Delta = \frac{\max(x_{n}) - \min(x_{n})}{n_{\text{bin}}}$$
(16)

where Δ represents the consistent gap used for signal discretization, while $n_{\rm bin}$ defines the granularity of the discrete state representation in the Markov model analysis.

Analyzing state sequences frequently involves calculating transition frequencies between states using statistical methods. This process is facilitated by the Markov Transition Matrix (MTM), which maps out the frequencies of state transitions and is dented as N_{ij}^{MTM} .

$$N_{ij}^{MTM} = \sum_{n=1}^{N-1} \delta(S_n = i, S_{n+1} = j)$$
 (17)

where the Kronecker Delta function, $\delta(x, y)$, returns 1 if x and y are identical, and 0 otherwise. N represents the total number of states in the sequence S.

To determine a typical percentage threshold for the baseline of a frequency distribution, one must compute the aggregate of all elements within the matrix. The computation is carried out using the following expression:

$$\theta = \alpha \cdot \sum_{i=1}^{n} \sum_{j=1}^{n} N_{ij}^{MTM}$$
 (18)

where the variable α , set at 0.1, representing the proportion of normal transition occurrences relative to the overall frequency. Thus, α quantifies the share of transitions deemed typical or standard.

To mitigate the influence of routine transitions within the matrix, diagonal entries and their immediate neighbors that surpass a specified threshold θ are nullified, setting their values to zero. This modification results in a matrix that highlights only significant transitions. The detailed procedure is as follows:

$$N_{ij}^{MTM'} = \begin{cases} 0 & \text{if } i = j \\ 0 & \text{if } N_{ij}^{MTM} > \theta \\ N_{ij}^{MTM} & \text{if } i \neq j \text{ and } N_{ij}^{MTM} \leqslant \theta \end{cases}$$
(19)

Upon eliminating the normal elements, the state matrix undergoes normalization, resulting in the formation of the Markov Transition Probability Matrix (MTPM), denoted as P_{ij} . This matrix reflects the probability of transitioning from state i to state j. The formula for P_{ij} . is as follows:

$$P_{ij} = \frac{N_{ij}^{MTM'}}{\sum_{j=1}^{N} N_{ij}^{MTM'} - \left(1 + N_{ij}^{\theta}\right)}$$
(20)

where N_{ij}^{θ} indicates the count of standard transition in row *i* that surpass the predefined threshold θ .

Next, prominent probabilities P'_{ij} are selected, representing latent anomalous state transitions, These anomalous state transitions are recorded in a set A by the following equation:

$$A = \{(i,j) \mid P_{ij} > 0\}$$
 (21)

Subsequently, in the discretized signal, based on the recorded state transitions in set A, moments indicating the imminent occurrence of anomalies are determined. For transitions from lower bin regions to higher bin regions, representing an increase in signal amplitude, these are markers of anomalies about to occur. Conversely, transitions in the opposite direction indicate that anomalies have already occurred and should be disregarded. This leads to the formation of an anomalous moment set T, which can be expressed as:

$$T = \{t \mid S_t = i, S_{t+1} = j, (i, j) \in A, i < j\}$$
 (22)

where T represents the set of anomalous moments that are about to occur. S_t is the signal state at time t.

By mapping the moments in set T back to the corresponding time points in the original signal, the amplitudes of the next sampling point at these moments are recorded. These amplitudes form a preliminary set of anomalous amplitudes V, which can be denoted as:

$$V = \{ x(t+1) \mid t \in T \}$$
 (23)

Then, the newly defined threshold, τ_{markov} , is given by:

$$\tau_{\text{markov}} = \mu_V + 3\sigma_V \tag{24}$$

where μ_V and σ_V represent the mean and standard deviation of the estimated set of anomalies, respectively.

Finally, the STCLPR outlined in (4) can be improved by incorporating the Markov Latent Frequency Transition Peak Rate (MLFTPR), as represented by:

$$MLFTPR = \frac{1}{M} \sum_{n=0}^{M-2} \mathbb{1} \{ \tau_{\text{markov}} > \Delta x[n] \}$$

$$\cdot \mathbb{1} \{ \tau_{\text{markov}} > \Delta x[n+1] \}$$
(25)

The indicator function, denoted here by 1, assigns a value of 1 if its argument is positive, and 0 otherwise. $\Delta x[n]$ represents the absolute difference between the signal x and its next sample point. This function effectively acts as a binary switch, dependent on the positivity of its input.

2024 Global Reliability and Prognostics and Health Management

Upon conducting a thorough analysis of the Markov Latent Frequency Transition Peak Rate (MLFTPR) across the entire signal, the average value is computed to establish a detection threshold that identifies irregular boundaries and defines a robust window for capturing missed anomalies. Corresponding segments in the underlying signal are then modified to handle amplitude peaks. The objective is to mitigate the effects of anomalies, bolster signal reliability, and improve analytical effectiveness, while preserving the fundamental characteristics of the original signal. The following equations encapsulate these methods:

$$\lambda = \frac{1}{K} \sum_{k=0}^{K-1} MLFTPR[k]$$
 (26)

$$\Omega = \left\{ k \mid MLFTPR[k] > \gamma \cdot \lambda \right\}$$
 (27)

$$y_{lim}^{i} = L \cdot \overline{x}, i \in (k \cdot M, k \cdot M + h), \forall k \in \Omega$$
 (28)

The term y^i_{lim} demotes the limited signal amplitude perturbation, where Ω defines the boundaries of anomalies, γ acts as the averaging factor, and L sets the amplitude constraints. The average amplitude, \bar{x} , is computed over a segment of length M with a stride h.

IV. EXPERIMENTAL VALIDATION

A. Test Rig Setup and Data Acquisition

To validate the proposed methodology's effectiveness, the bearing vibration dataset was collected using a test rig, as depicted in Fig. 1. This test rig includes a three-phase induction motor, a torque meter, a gearbox, bearing housings A and B, rotors, and a hysteresis brake. The experimental bearing used is a standardized NSK bearing (NSK 6205 DDU), featuring a ball diameter (d) of 7.90 mm, a pitch diameter (D) of 38.5 mm, contact degree angle (θ) of zero degrees, and nine (N) number of balls. Consequently, the shaft frequency (f_s) was measured at 50.17 Hz, the fundamental train frequency (FTF) at 19.94 Hz, and the ball pass frequency inner (BPFI) at 272.07 Hz, the ball pass frequency outer (BPFO) at 179.43 Hz, and the ball spin frequency (BSF) at 234.19 Hz. The vibration signal is collected at a sampling frequency of 25600Hz.

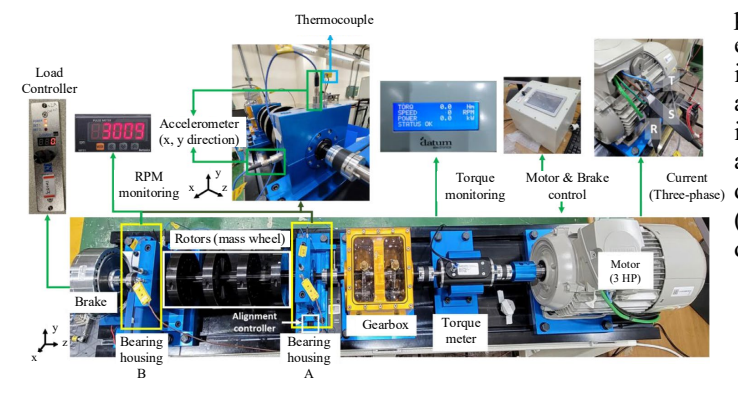


Figure 1. Experimental testing setup.

B. Experimental Validation and Comparative Analysis

The vibration signal illustrated in Fig. 2 exhibits random transient interferences. To effectively analyze this signal amid such noise, the employment of Discrete Wavelet Transform (DWT) as a preprocessing technique is selected. The DWT facilitates the decomposition of the signal while preserving its overall dynamics, as evidenced by the level 1 approximation coefficients shown in Fig. 2 (b). These coefficients demonstrate the retention of the signal's intrinsic features. Furthermore, the detailed coefficients at levels 1, 2, and 3, derived through the DWT, are presented in Fig. 2 (c)-(d).

Examining the high-frequency components at each level of the DWT reveals their sensitivity to rapid signal variations, which are crucial early indicators of potential significant events. Simultaneously, the low-frequency components provide insights into the fundamental structure and long-term trends of the signal. The application of low-pass filtering to the approximation coefficients enhances signal representation by eliminating minor perturbations. This process simplifies the signal's complexity and more accurately portrays its stable trends, as depicted in Fig. 3 (a) and Fig. 3 (b).

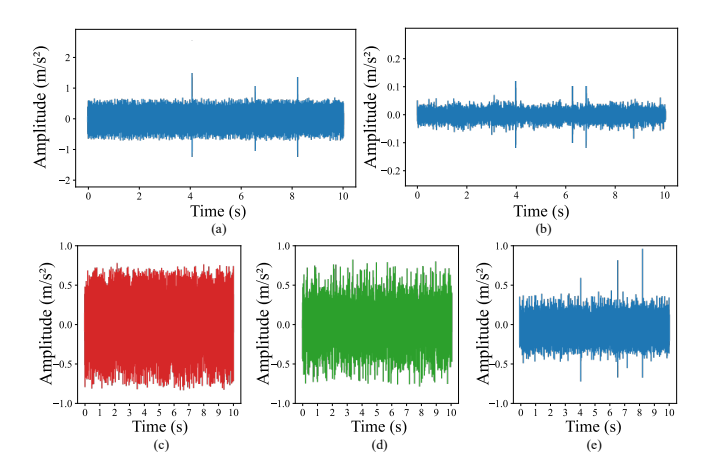


Figure 2. (a) Raw signal, (b) Level 1 approximation coefficient, (c) Detail coefficient (level 1), (d) Detail coefficient (level 2), and (e) Detail coefficient (level 3) in DWT.

A comparison between the original and retrieved signals is presented in Fig. 3 (c). The retrieved signal efficiently eliminates noise and accentuates significant external interferences, thereby enhancing the representation of anomalous signal transitions. By focusing on critical information, this method significantly improves the accuracy of anomaly detection. Subsequently, the signal is segmented into distinct states using equations (16)-(20). As depicted in Fig. 3 (d), this process results in discrete signals with clear interval distributions for both normal and noisy states.

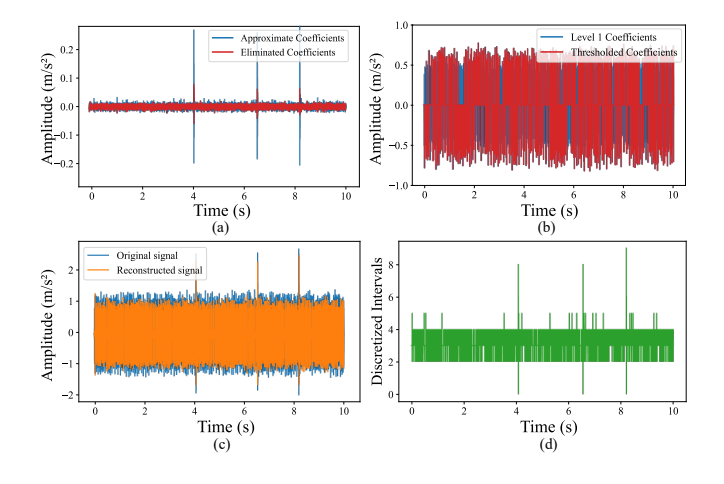


Figure 3. (a) Low-pass filtered approximation, (b) Thresholded detail coefficients, (c) Raw and reconstructed Signals, (d) Equidistant signal discretization.

To evaluate its effectiveness, the performance of the proposed method in monitoring signal transitions was compared with several established techniques, including Short-Time Energy (STE), Short-Time Kurtosis (STK), and Short-Time Zero Crossing Rate (STZCR), as illustrated in Fig. 4 (a)–(d).

The analysis reveals that the Short-Time Energy (STE) method, as depicted in Fig. 4 (a), which can find all the interference components, but there is still a small amount of interference. Similarly, the Short-Time Zero Crossing Rate (STZCR) approach, illustrated in Fig. 4 (b), fails to adequately differentiate transient noise interferences. The Short-Time Kurtosis (STK) method, shown in Fig. 4 (c), also encounters difficulties in recognizing interference components and is highly susceptible to significant noise from unaccounted signal elements. In contrast, the proposed MLFTPR, showcased in Fig. 4 (d), excels in accurately detecting all transient noise disturbances, without being affected by other undetected signal aberrations.

Fig. 5 provides a graphical representation of the frequency and probability distributions of Markov signals through dual heatmaps. In particular, Fig. 5 (a) presents the heatmap of Markov signal frequencies, illuminating the periodicity of state transitions. Here, intensely colored cells along the diagonal indicate a predominant persistence of states, signaling system resilience and the predictability of the signals. Bright spots off the diagonal represent state transitions, revealing the signal's dynamism and potential indicators of significant events or anomalies. Dark zones, bordered in white, represent rare or anomalous transitions, with the thickness of the borders correlating to the rarity of these occurrences. By modifying the heatmap to exclude high-frequency self-transitions on the diagonal and reduce off-diagonal high-frequency transitions, a normalized transition probability matrix is obtained, as displayed in Fig. 5 (b). This modification highlights lowerfrequency transitions, thereby enhancing the matrix's dynamic range. Consequently, this refined heatmap facilitates a more sensitive detection of subtle changes or transition patterns that might otherwise be overlooked in the frequency matrix.

Combining Fig. 3 (d) and Fig. 5 (b), we can get a series of possible anomaly points. According to (24), we can get the real anomaly points.

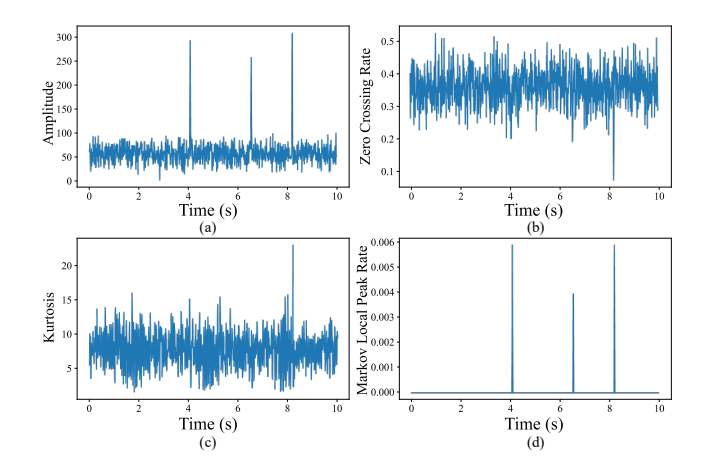


Figure 4. (a) STE, (b) STZCR, (c) STK, and (d) MLFTPR.

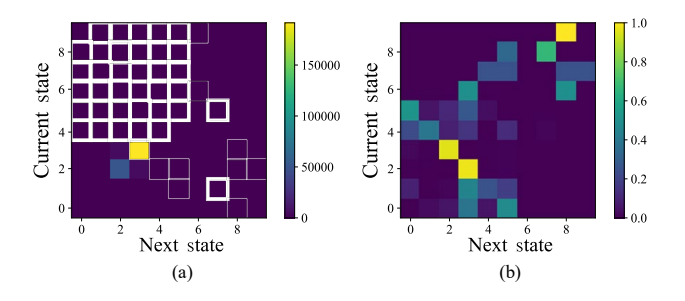


Figure 5. (a) Markov signal frequencies heat-map, (b) Scaled Markov signal probability heat-map.

As previously discussed, the proposed MLFTPR metric has demonstrated efficacy in identifying irregularities associated with external transient noises. This method exhibits robustness against such disruptions, thereby affirming the strength of the vibration signal in resisting external transient impacts. Furthermore, the incorporation of an amplitude-limiting component mitigates potential amplitude interferences, thereby enhancing the accuracy of fault identification.

The capability of this mechanism in controlling disturbance amplitudes is clearly illustrated in Fig. 6 (a), and Fig. 6 (b). Through the states in the transition matrix and the discretized signal, the moment preceding the occurrence of anomalies is estimated. Based on the corresponding position and amplitude in the original signal, a threshold $\tau_{\rm markov}$ is determined to distinguish between normal and anomalous behavior in low-probability transitions.

In the comparative case study, the Kurtogram [10] and Infogram [16] are employed as benchmark techniques. The analysis focuses on a raw bearing vibration signal, which is naturally susceptible to interference from external transient noise.. Various methods are implemented to mitigate post-interference effects and restrict amplitude interference in this

signal. After post-processing, the signals undergo analysis through demodulation band selection and envelope analysis.

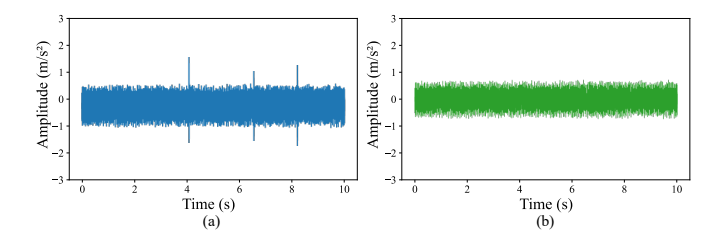


Figure 6. (a) Signals with interference, (b) Vibration signal with interference suppression.

The results of the demodulation band selection for the original vibration signal are illustrated in Fig. 7 (a) and Fig. 8 (a). Further analysis using Squared Envelope Spectrum (SES) [10] and Logarithmic Envelope Spectrum (LES) [16] are shown in Fig. 7 (b), Fig. 7 (c), Fig. 8 (b), and Fig. 8 (c). The Kurtogram identified a filtered central frequency and bandwidth of [400Hz, 800Hz], while the Infogram method yields a different set, with a central frequency and bandwidth of [800Hz, 533.3333Hz]. A closer analysis of the envelope results in Fig. 7 (b) and Fig. 8 (c) reveals a notable discrepancy—the absence of the characteristic bearing frequency. This observation contrasts with theoretical predictions, where the bearing's characteristic frequency should be identified as $f_i = 272.07$ Hz.

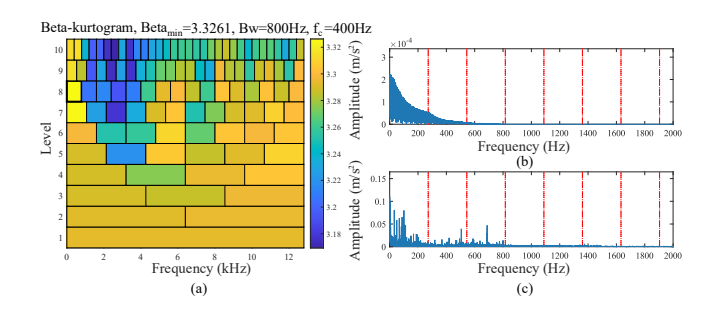


Figure 7. Raw signal affected by external transient noise interference: (a) Demodulation band determination via beta-Kurtogram, (b) Squared envelope spectrum, (c) Envelope spectrum in logarithmic scale.

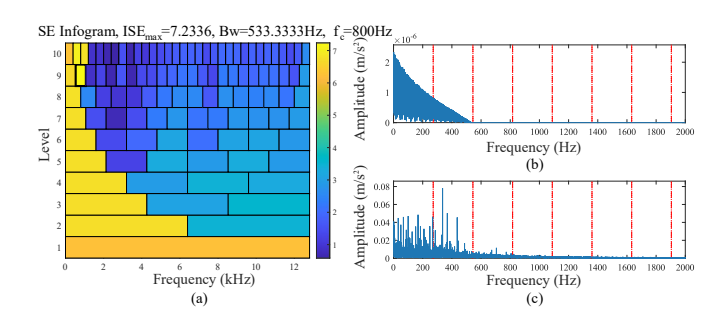


Figure 8. Raw signal affected by external transient noise interference: (a) Demodulation band determination via Infogram, (b) Squared envelope spectrum, (c) Envelope spectrum in logarithmic scale.

Fig. 9 (a) and Fig. 10 (a) demonstrate the effects of selecting various demodulation bands and conducting envelope analysis

on signals after amplitude interference limitation [22] and interference suppression. In contrast, Fig. 9 (b), Fig. 9 (c), Fig. 10 (b), and Fig. 10 (c) present envelope analyses conducted with the SES and LES methods. The derived parameters for the filtered central frequency and bandwidth are [1600Hz, 1066.6667Hz] for the first set and [2400Hz, 1600Hz] for the second set.

A thorough review of the envelope analysis results, depicted in Fig. 9 (b), Fig. 9 (c), Fig. 10 (b), and Fig. 10 (c), indicates a clear identification of characteristic frequencies, such as f_i , $2f_i$, and $3f_{ii}$. These findings are crucial in substantiating the effectiveness of the proposed method in monitoring signal state transitions, which is particularly relevant for bearing diagnostics environments with significant external noise challenges.

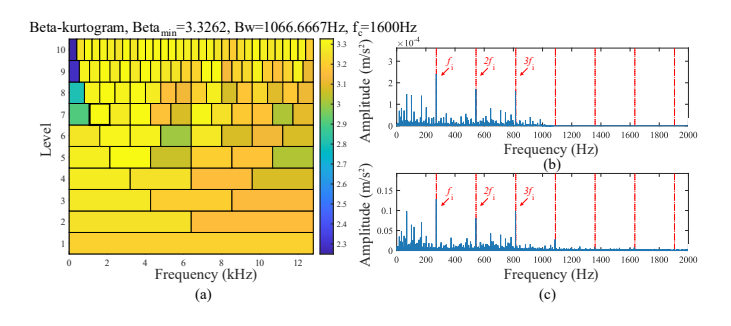


Figure 9. Signal after post-interference suppression and amplitude limitation:
(a) Demodulation band determination via beta-Kurtogram, (b) Squared envelope spectrum, (c) Envelope spectrum in logarithmic scale.

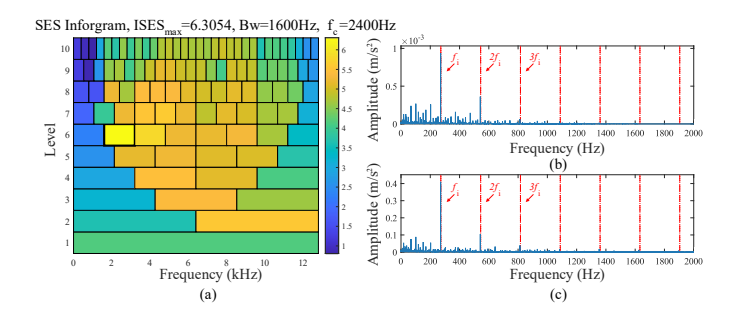


Figure 10. Signal after post-interference suppression and amplitude limitation:
(a) Demodulation band determination via Infogram, (b) Squared envelope spectrum, (c) Envelope spectrum in logarithmic scale.

V. CONCLUSION

This research introduces the Markov Latent Frequency Transition Peak Rate (MLFTPR) methodology, designed to overcome diagnostic challenges caused by environmental disruptions in rolling bearings. By vigilantly tracking state transitions and identifying anomalous signals, MLFTPR enhances fault diagnosis in noise-cluttered environments. Its amplitude interference control improves the accuracy of demodulation band selection, thus boosting diagnostic precision. Experimental results demonstrate MLFTPR's resilience against transient noise, proving it superior to traditional techniques. In subsequent work, the effect of the number of bins in (15) on the result can be discussed.

REFERENCES

- [1] Z. Ren, T. Lin, K. Feng, Y. Zhu, Z. Liu, and K. Yan, "A Systematic Review on Imbalanced Learning Methods in Intelligent Fault Diagnosis," *IEEE Transactions on Instrumentation and Measurement*, vol. 72, no. 3508535, pp. 1–35, 2023.
- [2] P. Chen, Y. Li, K. Wang, M. J. Zuo, P. S. Heyns, and S. Baggeröhr, "A threshold self-setting condition monitoring scheme for wind turbine generator bearings based on deep convolutional generative adversarial networks," *Measurement*, vol. 167, p. 108234, 2021.
- [3] P. Chen, Y. Li, K. Wang, and M. J. Zuo, "An automatic speed adaption neural network model for planetary gearbox fault diagnosis," *Measurement*, vol. 171, p. 108784, 2021.
- [4] P. Chen, K. Wang, M. J. Zuo, and D. Wei, "An ameliorated synchroextracting transform based on upgraded local instantaneous frequency approximation," *Measurement*, vol. 148, p. 106953, 2019.
- [5] C. Li, D. Cabrera, J. V. de Oliveira, R.-V. Sanchez, M. Cerrada, and G. Zurita, "Extracting repetitive transients for rotating machinery diagnosis using multiscale clustered grey infogram," *Mechanical Systems and Signal Processing*, vol. 76–77, pp. 157–173, 2016.
- [6] D. Ruan, J. Wang, J. Yan, and C. Guhmann, "CNN parameter design based on fault signal analysis and its application in bearing fault diagnosis," ADVANCED ENGINEERING INFORMATICS, vol. 55, p. 101877, Jan. 2023,
- [7] H. Fang et al., "You can get smaller: A lightweight self-activation convolution unit modified by transformer for fault diagnosis," ADVANCED ENGINEERING INFORMATICS, vol. 55, p. 101890, Jan. 2023,
- [8] R. B. Randall and J. Antoni, "Rolling element bearing diagnostics—A tutorial," *Mechanical systems and signal processing*, vol. 25, no. 2, pp. 485–520, 2011.
- [9] R. F. Dwyer, "A technique for improving detection and estimation of signals contaminated by under ice noise," *The Journal of the Acoustical Society of America*, vol. 74, no. 1, pp. 124–130, 1983.
- [10] J. Antoni and R. B. Randall, "The spectral kurtosis: application to the vibratory surveillance and diagnostics of rotating machines," *Mechanical Systems and Signal Processing*, vol. 20, no. 2, pp. 308–331, 2006.
- [11] J. Antoni, "Fast computation of the kurtogram for the detection of transient faults," *Mechanical Systems and Signal Processing*, vol. 21, no. 1, pp. 108–124, 2007.

- [12] Y. Lei, J. Lin, Z. He, and Y. Zi, "Application of an improved kurtogram method for fault diagnosis of rolling element bearings," *Mechanical Systems and Signal Processing*, vol. 25, no. 5, pp. 1738–1749, 2011.
- [13] P. Borghesani and M. R. Shahriar, "Cyclostationary analysis with logarithmic variance stabilisation," *Mechanical Systems and Signal Processing*, vol. 70–71, pp. 51–72, Mar. 2016.
- [14] T. Barszcz and A. Jabł-oński, "A novel method for the optimal band selection for vibration signal demodulation and comparison with the Kurtogram," *Mechanical Systems and Signal Processing*, vol. 25, pp. 431–451, 2011.
- [15] B. Chen et al., "Product envelope spectrum optimization-gram: An enhanced envelope analysis for rolling bearing fault diagnosis," MECHANICAL SYSTEMS AND SIGNAL PROCESSING, vol. 193, p. 110270, Jun. 2023,
- [16] J. Antoni, "The infogram: Entropic evidence of the signature of repetitive transients," *Mechanical Systems and Signal Processing*, vol. 74, pp. 73– 94, 2016.
- [17] P. A. Schirmer and I. Mporas, "Energy disaggregation from low sampling frequency measurements using multi-layer zero crossing rate," in ICASSP 2020-2020 IEEE International Conference on Acoustics, Speech and Signal Processing (ICASSP), IEEE, 2020, pp. 3777–3781.
- [18] S. Alimi and O. Awodele, "Voice activity detection: Fusion of time and frequency domain features with a svm classifier," *Comput. Eng. Intell. Syst*, vol. 13, no. 3, pp. 20–29, 2022.
- [19] B. Chen, Y. Hu, L. Wu, and H. Li, "Partial Discharge Pulse Extraction and Interference Suppression Under Repetitive Pulse Excitation Using Time-Reassigned Multi-Synchrosqueezing Transform," *IEEE Transactions on Instrumentation and Measurement*, pp. 1–9, 2023.
- [20] I. Daubechies and W. Sweldens, "Factoring wavelet transforms into lifting steps," *Wavelets in the Geosciences*, pp. 131–157, 2005.
- [21] I. Daubechies, "The wavelet transform, time-frequency localization and signal analysis," *IEEE transactions on information theory*, vol. 36, no. 5, pp. 961–1005, 1990.
- [22] P. Chen, Y. Wu, C. Xu, Y. Jin, and C. Zhou, "Markov Modeling of Signal Condition Transitions for Bearing Diagnostics under External Interference Conditions," *IEEE Transactions on Instrumentation and Measurement*, vol. 73, no. 3518308, pp. 1–8, 2024.